3D Turbulence Simulations of the Impact of Plasma Rotation on Stiffness Level

S. Sugita[1,2,3], P. Beyer[1,2], G. Fuhr[1,2], F. Jaulmes[1,2], S. Benkadda[1,2], X. Garbet[4], M. Yagi[2,5,6], S.-I. Itoh[2,5], K. Itoh[2,7]

[1] *IIFS, CNRS-Université de Provence, Marseille, France*

[2] *France-Japan Magnetic Fusion Laboratory, LIA 336 CNRS, Marseille, France*

[3] *IGSES, Kyushu University, Kasuga, Japan*

[4] *CEA/IRFM, St. Paul-Lez-Durance, France*

[5] *RIAM, Kyushu University, Kasuga, Japan*

[6] *JAEA, Naka, Japan*

[7] *NIFS, Toki, Japan*

1. Introduction

Recent experiments at JET have shown that driving a large-scale rotation of the plasma improves confinement. In particular, the so-called stiffness level of the ion temperature profile is found to decrease with plasma rotation [1]. The level of stiffness characterizes the fact that above a critical value of the ion temperature inverse gradient length ($R/L_{T_i} = R\left|\nabla T_i\right|/T_i$, where R indicates the tokamak major radius) the ion heat flux increase strongly with R/L_{T_i}. This behavior is attributed to turbulent transport.

In this work we report on 3D turbulent simulations in a flux driven configuration (i.e. with self consistent profile evolution), revealing the behavior of the pressure gradient as a function of the imposed total energy flux. Different scenarios with respect to plasma rotation (turbulence driven rotation, artificially suppressed or imposed rotation) are studied.

2. Model and Simulation Conditions

The two field reduced MHD equations are solved to reproduce the plasma edge turbulence in the Tokamak geometry [2]. The following equations are for the normalized electrostatic potential ϕ and pressure p.

$$\frac{\partial}{\partial t}\nabla_\perp^2\phi + \left[\phi, \nabla_\perp^2\phi\right] = -\nabla_{\|0}\phi - \mathbf{G}p + \nu\nabla_\perp^4\phi, \tag{1}$$

$$\frac{\partial}{\partial t}\nabla_\perp^2\phi_{00} + \left[\phi, \nabla_\perp^2\phi_{00}\right] = -\nabla_{\|0}\phi - \mathbf{G}p + \nu\nabla_\perp^4\phi + \mu\nabla_\perp^2\left(\phi_{\mathrm{imp}} - \phi_{00}\right), \tag{2}$$

$$\frac{\partial p}{\partial t} + [\phi, p] = \delta_{\mathrm{c}}\mathbf{G}\phi + \chi_\| \nabla_{\|0}^2 p + \chi_\perp \nabla_\perp^2 p + S(r), \tag{3}$$

where $[f,g] = (\partial f/\partial x)(\partial g/\partial y) - (\partial f/\partial y)(\partial g/\partial x)$ is the Poisson bracket. $\nabla_\perp^2 = \partial^2/\partial x^2 + \partial^2/\partial y^2$ and $\nabla_{\|0} = \partial/\partial z - (k_z/q)(\partial/\partial y)$ are the gradients perpendicular and parallel to the field

line.

The curvature operator is $\mathbf{G} = \sin(k_y y)(\partial/\partial x) + \cos(k_y y)(\partial/\partial y)$. ν indicates the viscosity, $\chi_{\|}$ and $\chi_{\perp}$ are parallel and perpendicular heat diffusivities. δ_c is the parameter that is related to the ratio between the pressure gradient length and the major radius R_0. Time is normalized by the resistive interchange time $\tau_{\rm int} = (R_0 L_p/2)^{1/2}/c_s$, where c_s is the sound speed, and L_p is the pressure gradient length. Perpendicular length is normalized by the resistive ballooning length $\xi_{\rm bal} = (\rho\eta_{\|}/\tau_{\rm int})^{1/2} L_s/B_0$, where ρ is the mass density, $\eta_{\|}$ is the parallel resistivity, and parallel length is normalized to the magnetic shear length L_s. The model equation is solved numerically by the finite difference method in the radial direction and by a Fourier expansion in the poloidal and toroidal direction. In the (m,n) space, all modes are simulated except for the $(n=0, m>0)$ modes to keep the neoclassical terms consistent (especially for $(1,0)$ mode) [3].

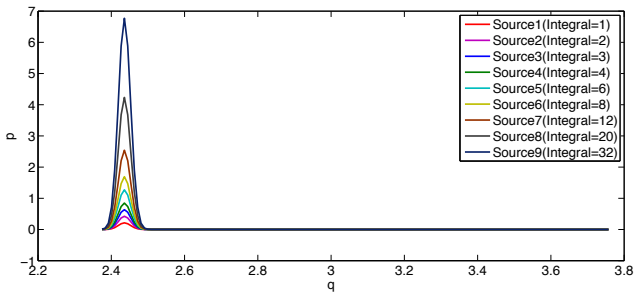

Figure 1: Radial profile of the pressure source $S(r)$.

Assuming a monotonically increasing safety factor $q(r)$, the simulations cover a domain between $q = 2.5$ and $q = 3.5$. The regions $q < 2.5$ and $q > 3.5$ are used for a dumping buffer. Gaussian type pressure source is introduced in the buffer region. We vary the amplitude of the source profile such that the integral, i.e. the total energy flux varies from 1 to 32 (see Fig. 1). The simulations are performed for the following three scenarios concerning the poloidal rotation: artificially suppressed case (ref. case), spontaneous rotation case (spo. case), and artificially imposed rotation case (imp. case).

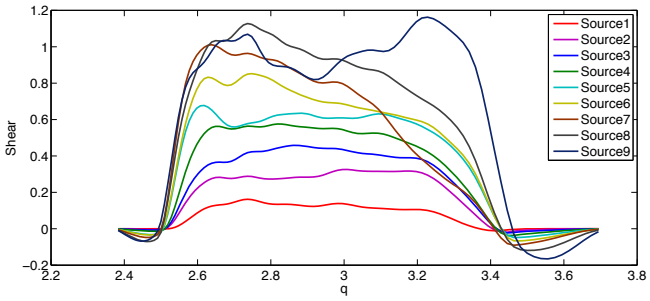

Figure 2: Time averaged radial profiles of the velocity shear in the spo. case. Source variations correspond to fig. 1.

3. Simulation Results

Nonlinear simulations are performed until a quasi-steady state is reached and the temporal and spatial (poloidal and toroidal) averages are taken in that state.

Figure 2 shows the radial profile of the $\mathbf{E} \times \mathbf{B}$ velocity shear in the self consistent case with spontaneous rotation. Evidently, the shear amplitude is increasing with the total energy flux. Alternatively, we impose different rotation velocities with broad velocity shears and a variety of amplitudes (imp. case, fig. 3).

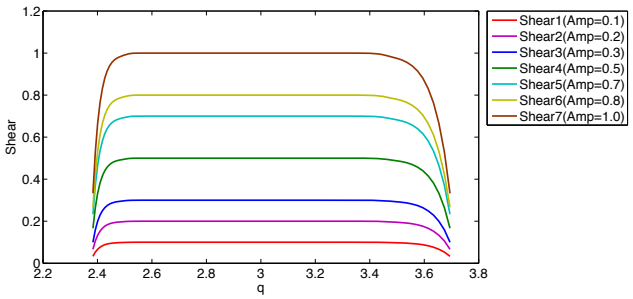

Figure 3: Radial profiles of the imposed velocity shear in the imp. case.

In figures 4 to 5 the mean pressure gradient is plotted versus the total imposed energy flux. In fig. 4, the spo. case is compared to the ref. case. In fig. 5, varies of imp. cases are compared to the ref. case. It is clearly shown that the rotation keeps the pressure gradient steep. For the fitting curve, we use the gyro-Bohm type relation between the total energy flux and the pressure gradient, parameterized by the stiffness level, and the critical gradient (eq. (4)) [1].

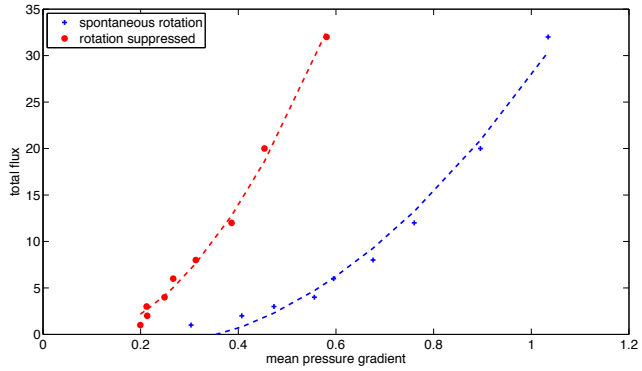

Figure 4: Mean pressure gradient versus total imposed flux with fitting curves for ref. case and spo. case.

$$Q_{\mathrm{tot}} = Q^{\mathrm{res}} + \chi_{\mathrm{g\text{-}B}} q^{1.5} \frac{\tau_{\mathrm{int}}}{\xi_{\mathrm{bal}}^2} \chi_{\mathrm{s}} \frac{\mathrm{d}p}{\mathrm{d}r} \left(\frac{\mathrm{d}p}{\mathrm{d}r} - \left. \frac{\mathrm{d}p}{\mathrm{d}r} \right|_{\mathrm{crit}} \right), \tag{4}$$

where Q_{tot} is the total imposed pressure, Q^{res} the residual flux, including the neoclassical flux, $\chi_{\mathrm{g\text{-}B}} = T_e \rho_i / (BR)$ the gyro-Bohm coefficient, q the safety factor, χ_{s} the stiffness level, and $\mathrm{d}p/\mathrm{d}r|_{\mathrm{crit}}$ the threshold of the pressure gradient. The fitting gives χ_{s} and $\mathrm{d}p/\mathrm{d}r|_{\mathrm{crit}}$ for each curve. The fitting is done in the statistically stationary state (not the relaxation oscillation or simple diffusion).

Figure 6 shows the stiffness level χ_s versus the velocity shear amplitude and fig. 7 shows the critical gradient $\mathrm{d}p/\mathrm{d}r|_{\mathrm{crit}}$ versus the velocity shear amplitude, both in the imp. case. They are given by the fitting curve in fig. 5. The critical gradient is linearly proportional to the strength of the velocity shear, but the tendency of the stiffness level is not clear.

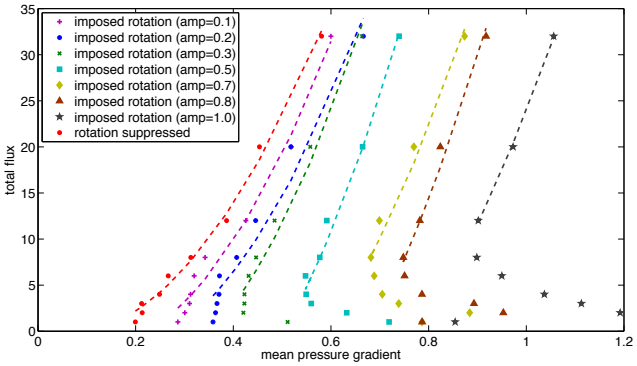

Figure 5: Mean pressure gradient versus total imposed flux with fitting curves for ref. case and imp. cases.

In conclusion, the slope of the flux-vs-grad-p-curve is clearly lower in the presence of turbulence generated rotation (spo. case) compared to a ref. case where rotation is artificially suppressed (Fig. 4). However, for different amplitudes of imposed rotation (imp. cases), the slopes are similar, i.e. the stiffness does not change significantly, only the critical gradient changes. Therefore, the change in the slope with self-generated rotation has to be attributed to the fact that the rotation amplitude itself is increasing with the total energy flux.

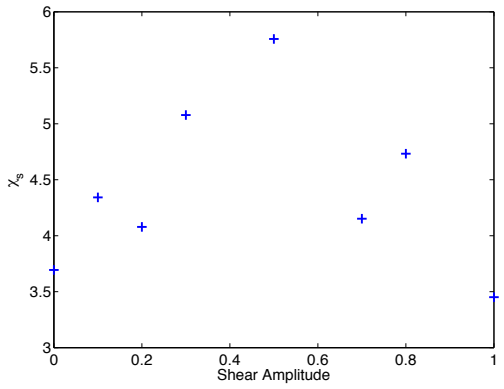

Figure 6: Stiffness level versus imposed shear amplitude.

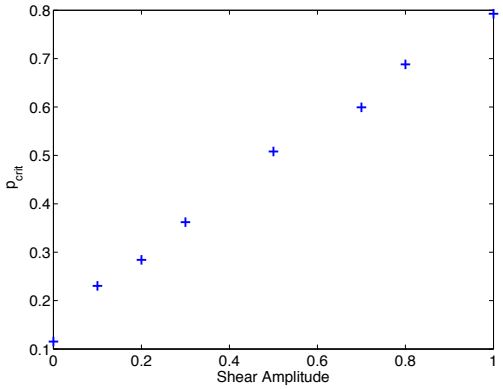

Figure 7: Critical gradient of the pressure versus imposed shear amplitude.

References

[1] P. Mantica *et al.*, Phys. Rev. Lett. **102**, 175002 (2009)

[2] P. Beyer *et al.*, Plasma Phys. Control. Fusion **49**, 507 (2007)

[3] G. Fuhr *et al.*, Phys. Rev. Lett. **101**, 195001 (2008)